J. Fluid Mech. (1992), *vol.* 237, *pp.* 189–208
Printed in Great Britain

Secondary motion of fully developed oscillatory flow in a curved pipe

By K. SUDO[1], M. SUMIDA[2] AND R. YAMANE[3]

[1] Department of Mechanical Engineering, Hiroshima University, Kagamiyama, Higashihiroshima, 724, Japan

[2] Department of Mechanical Engineering, Yonago National College of Technology, Hikona-cho, Yonago, Tottori, 683, Japan

[3] Department of Mechanical Engineering, Tokyo Institute of Technology, Ookayama, Meguro-ku, Tokyo, 152, Japan

(Received 1 May 1990 and in revised form 23 September 1991)

Experimental and numerical studies were made of the secondary flow induced in fully developed oscillatory laminar flow in a curved circular pipe. Photographs of traces of nylon particles suspended in water were taken systematically with Womersley numbers $\alpha = 5.5 \sim 28$ and oscillatory Dean numbers $D = 40 \sim 500$. The secondary flow velocity component and the location of the vortex eye were obtained from the photographs. The experimental results were checked with the numerical ones and the variations of the secondary flow pattern with the Dean and Womersley numbers were analysed based on both results. These results suggest that secondary flows can be classified into five patterns.

1. Introduction

The complex flow in a curved pipe is of interest not only as a scientific problem but also in practical engineering problems such as the design of heat exchangers and chemical reactors.

In earlier studies, Dean (1927, 1928) analysed laminar steady flow in a circular curved pipe for small values of Dean number by the perturbation method. His studies were followed by the investigations of Topakoglu (1967), Sankaraiah & Rao (1973), Li (1976) and Van Dyke (1978) with the help of the successive approximation. Adler (1934) and others (e.g. Barua 1963; Ito 1969; Smith 1976) analysed approximately the high-Dean-number flows by applying the concept of boundary-layer theory and proved that the method is effective for estimating the resistance factor. Since the development of electronic computers, interesting numerical results for intermediate Dean numbers have been presented by Truesdell & Adler (1970) and others (e.g. Akiyama & Cheng 1971; Kalb & Seader 1972; Austin & Seader 1973; Tarbell & Samuels 1973; Greenspan 1973; Collins & Dennis 1975). Though the studies of steady flow are not reviewed in detail here, it is sufficient to note that many studies have been made for a wide range of Dean numbers.

The most recent interest in curved pipe flow has been concentrated on unsteady flow with reference to physiological problems. As the phenomenon of unsteady flow is very complicated, oscillatory or pulsatory flow, being the most simple case, has been chosen in many studies. There are detailed reviews of unsteady curved pipe flow in the works of Berger, Talbot & Yao (1983) and Chang & Tarbell (1985), but here only works on purely oscillatory flow relevant to the present study are reviewed.

Lyne (1970) developed a perturbation theory, for small values of the frequency parameter $\beta(=\sqrt{2}/\alpha)$, for the flow under a sinusoidally varying pressure gradient and obtained the asymptotic solutions for two cases of $R_s \ll 1$ and $R_s \gg 1$, where α is the Womersley number and R_s the Reynolds number of secondary flow. He showed that two couples of vortices are induced for sufficiently high Womersley numbers. The new secondary flow found by Lyne was confirmed by Zalosh & Nelson (1973) and Mullin & Greated (1980) by using the perturbation method which was similar to that employed in Dean's work (1927, 1928) for steady flow. A more recent study (Eckmann & Grotberg 1988), using a regular perturbation method, which was conducted in connection with a mass transfer problem, also verified Lyne's prediction. Christov & Zapryanov (1980) also proved the formation of Lyne circulation by solving numerically the governing equations, simplified by the assumption of a large curvature ratio of the pipe.

The interesting nature of the secondary flow stimulated many experimentalists. Lyne (1970) injected dye into the flow through a clear plastic pipe and viewed the streak at $\alpha = 28$. The photographs taken suggested that there exist four vortices, that is, two couples of vortices in a cross-section. Munson (1975) observed the movement of the streak of dye for the range $0.7 \lesssim \alpha \lesssim 32$ and measured the secondary flow velocities at the pipe-axis on the basis of the picture. Bertelsen (1975) and Bertelsen & Thorsen (1982) succeeded in taking pictures of Lyne circulation by an aluminium-powder tracer technique.

Unfortunately, however, all of the visualization experiments have been concerned with the flows for low Dean numbers, that is, $D \lesssim 10$ and extreme Womersley numbers, and only confirmed the theoretical results qualitatively. Therefore, useful results have not been obtained for practical problems, in which the Dean number goes up to the order of 100 and the Womersley number shows moderate values. For example, in blood flow through an aorta, which has led researchers to study the oscillatory flow in a curved pipe, the Womersley number α has values of 8–16, at which the flow presents different characteristics from the Dean-type motion for low Womersley numbers and the Lyne-type one for high Womersley numbers. Thus it is hoped to obtain much useful information for practical flows such as the flow in the aorta.

The purpose of this study is to treat the problem of fully-developed, laminar oscillatory flow in a circular curved pipe by experimental and numerical means and especially to obtain the knowledge of secondary flow in a wide range of Dean and Womersley numbers.

2. Experimental apparatus and procedures

The schematic diagram of the experimental apparatus employed in this study is shown in figure 1. The pipe system consists of a helical pipe connected to two straight pipes at its inlet and exit and filled with water. The helical pipe with a circular cross-section is made of a transparent glass tube with a refractive index of 1.46, and is turned into three loops with small pitch. The dimensions of the pipe are as follows: inside diameter, $2a$, is 14.1 mm and outside diameter 18.0 mm; radius of helix $R = 53.3$ mm; curvature ratio of the pipe $Rc(= R/a) = 7.6$ (see figure 2). One of five piston pumps with a scotch yoke mechanism, which is suitably chosen according to the experimental conditions, is attached to one end of the pipe and driven harmonically by a variable speed motor. The diameter of each pump is 6, 10, 15, 20 and 28 mm and the stroke of the piston lies in the range 0–100 mm. The pipe is put

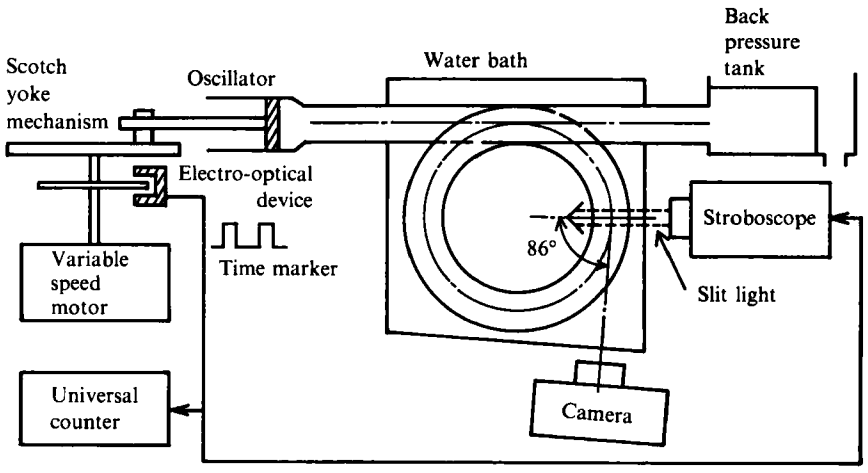

FIGURE 1. Experimental apparatus, showing the flow generator with the scotch yoke mechanism, the pipe system, the back pressure controller and visualizing and photographing devices.

in a transparent box-type bath, in which water circulates, so as to reduce light refraction due to the pipe curvature. A desirable flow-rate in sinusoidal waveform is obtained by adjusting the variable speed motor and choosing the appropriate piston pump, which is expressed in terms of the axial velocity averaged over the cross-section:

$$w_m = \tilde{w}_m \sin \Theta, \tag{1}$$

where $\Theta (= \omega t)$ is the phase angle, ω the angular frequency of oscillation, t the time and $\tilde{w}_m$ the amplitude of w_m.

The secondary flow observations are made by means of a tracer method. Approximately spherical nylon particles having an average diameter of about 90 μm are chosen as tracers because their specific gravity is about unity and they reflect the illuminated light efficiently from their surface. Measurements are made at streamwise station $\phi = 450°$ (one and a quarter loops), ϕ being the angle measured along the z-axis from the helical pipe inlet. The fluid layer to be recorded is illuminated by a sheet of stroboscopic light and the paths of the tracer particles irradiated are photographed from the direction shown in figure 1. The stroboscopic illumination is repeated in synchronization with a time-marker signal which indicates the position of the piston every one degree.

The photographic recordings are obtained by the following alternative methods, according to the distance s of which nylon particle makes a run in the cross-section during a cycle of the oscillatory motion of the fluid. For the case of large s (that is, $s \gtrsim 0.2a$) where the Womersley number α is low, the fluid layer is illuminated with a sequence of 3–5 irradiations in the vicinity of a fiducial phase, e.g. $\Theta = 0°$ which is the maximum accelerative phase or $\Theta = 90°$ which corresponds to the maximum flow rate in a cycle. In this case, the frequency of irradiation is 5–50 Hz and the irradiative phase interval $\Delta\Theta$ is 2–15°. The symbol ① is used to represent this method hereinafter. On the other hand, when s reduces with an increase of the Womersley number, it becomes harder to catch the streaks of the particles at a fiducial phase and its vicinity in one cycle. In such flows, the fluid in the central region of the pipe moves in the same phase with the piston pump and the axial velocity becomes uniform except near the wall. This means that the particles

Identification mark of experiment	D	α	Photographic recording method	$\Theta(\Delta\Theta)$ or Δt	Remarks (figure no.)	Secondary flow pattern
q	40	5.5	①	0° (10°)	5(q)	I
r	41	10.3	②	1 T_p	5(r)	II
a	98	5.4	①	0° (4°)	3(a), 5(a)	I
b	98	5.4	①	90° (2°)	3(b)	I
c	97	10.5	②	1 T_p	3(c), 5(c)	II
d	100	14.0	②	2 T_p	3(d), 5(d)	IV
e	98	17.6	②	4 T_p	3(e), 5(e)	V
s	97	28.1	②	15 T_p	5(s)	V
f	194	5.6	①	15° (4°)	3(f), 5(f)	I
g	194	5.6	①	90° (2°)	3(g)	I
h	195	9.9	①	0° (5°)	3(h), 5(h)	I
i	202	13.5	②	1 T_p	3(i), 5(i)	III
j	201	17.7	②	1 T_p	3(j), 5(j)	V
k	193	28.0	②	15 T_p	3(k), 5(k)	V
t	282	5.4	①	0° (4°)	5(t)	I
u	298	9.9	①	0° (4°)	5(u)	I
l	290	13.6	①	0° (10°)	3(l), 5(l)	II
m	282	19.5	②	1 T_p	3(m), 5(m)	IV
v	286	28.0	②	3 T_p	5(v)	V
w	345	17.6	②	1 T_p	5(w)	III
y	417	27.4	②	1 T_p	5(y)	V
n	515	5.6	①	0° (5°)	3(n), 5(n)	I
x	487	14.0	①	0° (6°)	5(x)	I
o	493	17.9	①	0° (15°)	3(o), 5(o)	II
p	491	28.2	②	1 T_p	3(p), 5(p)	V
				Curvature ratio $Rc = 7.6$		

TABLE 1. Details of the experimental conditions. Θ denotes the phase angle when the photograph is taken and $\Delta\Theta$ the interval of the stroboscope irradiation. Δt is the real time interval between the irradiations and T_p the period of the oscillatory motion.

illuminated at a given phase Θ will still exist in the same cross-section after one cycle, that is, at the phase of $(\Theta + 2\pi)$. For this case of small s (that is, $s \lesssim 0.14a$), therefore, one flash of the stroboscope is given at 1–15 cycles, the flash interval of the stroboscope corresponding to the real time interval Δt of 0.25–5 s. One photographic recording is obtained by 5–25 repetitions of flash. This procedure is called method ②. In conclusion, the instantaneous velocities averaged at the fiducial phase and its vicinity are obtained in method ① and the time-averaged velocities over one cycle are given in method ②, respectively.

Using the above-stated methods, the instantaneous or time-averaged velocity vectors of the secondary flow can be readily determined independent of the time exposing a film or the time necessary for tracer particles to pass through the section illuminated.

Though the optical distortion due to the pipe curvature is reduced by putting the pipe in the water bath, it is still necessary to take care in photographing the outer region of the cross-section. In this recording system, the length along the x-axis from the pipe-axis to the wall observed by the camera is different in outer and inner bends; the length to the inner bend is longer than that to the outer bend, the ratio being

about 1:0.92. This is taken into account when the velocity vectors of the secondary flow are determined from the photographs.

The preliminary measurements made in the cross-section at $\phi = 810°$ (two and a quarter loops) prove that the flow is fully developed at $\phi = 450°$.

The experiments were carried out in the range of Womersley numbers $\alpha(= a[\omega/\nu]^{\frac{1}{2}})$ of 5.5–28 (in other words, frequencies of 0.12–3.4 Hz) and Dean numbers $D(= Re[a/R]^{\frac{1}{2}})$ of 40–500 in order to study systematically the secondary-flow characteristics; the Dean number corresponds to the Reynolds number $Re(= 2a\tilde{w}_m/\nu)$ of 110–1400, $\tilde{w}_m$ taking the values of 1–13 cm/s, where ν is the kinematic viscosity of the fluid. Details of the experimental conditions are given in table 1.

3. Numerical analysis

A system of coordinates as shown in figure 2 is chosen for the analysis. The flow in a curved pipe is assumed to be a fully-developed laminar flow of incompressible viscous fluid, the pipe itself being coiled in a curvature radius R. The velocity components corresponding to coordinates (x, y, z) are (u, v, w) which are independent of z. All dimensions are made dimensionless with reference to the pipe radius a. The velocities are non-dimensionalized with ν/a after the past numerical analyses (e.g. Truesdell & Adler 1970; Kalb & Seader 1972; Austin & Seader 1973). The other physical quantities can be made dimensionless by use of the density ρ and kinematic viscosity ν of the fluid.

Therefore, the following non-dimensional notations are introduced:

$$\left.\begin{aligned} &X = x/a, \quad Y = y/a, \quad Z = z/a, \quad r = r'/a, \quad Rc = R/a, \\ &U = au/\nu, \quad V = av/\nu, \quad W = aw/\nu, \quad P = a^2p/(\rho\nu^2), \\ &T = \nu t/a^2, \quad \Omega = \xi a^2/\nu, \quad \Psi = \psi/\nu, \end{aligned}\right\} \tag{2}$$

where ξ and ψ denote the vorticity and stream function of the secondary flow respectively; p is the pressure and r' and θ are radial and angular positions. The governing equations for the fluid motion in the toroidal coordinates (r, θ, Z) are given in terms of W, Ω and Ψ as follows:

$$\frac{\partial W}{\partial T} = \frac{\partial^2 W}{\partial r^2} + \frac{1}{r^2}\frac{\partial^2 W}{\partial \theta^2} + \left(A + \frac{1}{r} + \frac{1}{Hr}\frac{\partial \Psi}{\partial \theta}\right)\frac{\partial W}{\partial r} + \left(B - \frac{1}{H}\frac{\partial \Psi}{\partial r}\right)\frac{1}{r}\frac{\partial W}{\partial \theta} - \left\{\frac{1}{H^2} + \left(\frac{B}{H}\frac{\partial \Psi}{\partial r} - \frac{A}{H}\frac{1}{r}\frac{\partial \Psi}{\partial \theta}\right)\right\} W - \frac{Rc}{H}\frac{\partial P}{\partial Z}, \tag{3}$$

$$\frac{\partial \Omega}{\partial T} = \frac{\partial^2 \Omega}{\partial r^2} + \frac{1}{r^2}\frac{\partial^2 \Omega}{\partial \theta^2} + \left(A + \frac{1}{r} + \frac{1}{Hr}\frac{\partial \Psi}{\partial \theta}\right)\frac{\partial \Omega}{\partial r} + \left(B - \frac{1}{H}\frac{\partial \Psi}{\partial r}\right)\frac{1}{r}\frac{\partial \Omega}{\partial \theta} + \left\{\frac{1}{H^2} + \left(\frac{B}{H}\frac{\partial \Psi}{\partial r} - \frac{A}{H}\frac{1}{r}\frac{\partial \Psi}{\partial \theta}\right)\right\} \Omega + 2W\left(B\frac{\partial W}{\partial r} - \frac{A}{r}\frac{\partial W}{\partial \theta}\right), \tag{4}$$

$$H\Omega = \frac{\partial^2 \Psi}{\partial r^2} + \frac{1}{r^2}\frac{\partial^2 \Psi}{\partial \theta^2} + \left(\frac{1}{r} - A\right)\frac{\partial \Psi}{\partial r} - \frac{B}{r}\frac{\partial \Psi}{\partial \theta}, \tag{5}$$

where

$$\left.\begin{aligned} &H = Rc + r\sin\theta, \\ &A = \sin\theta/H, \quad B = \cos\theta/H. \end{aligned}\right\} \tag{6}$$

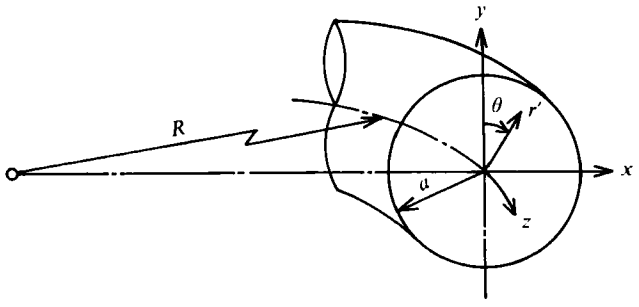

FIGURE 2. Coordinates of the curved circular-pipe section.

We now impose the following sinusoidal flow rate so as to correspond with the experimental condition;

$$Q = \int_{-\pi}^{\pi} \int_{0}^{1} W r \, \mathrm{d}r \, \mathrm{d}\theta = \pi \tilde{W}_{\mathrm{m}} \sin \Theta, \tag{7}$$

where Q is the dimensionless flow rate, that is, $Q = q/(\nu a)$.

The boundary conditions are derived from the physical considerations:

$$\left.\begin{aligned} &\frac{\partial W}{\partial \theta} = \Omega = \Psi = 0 && \text{at the } X\text{-axis} \quad (\theta = \pm \tfrac{1}{2}\pi), \\ &W = \Psi = 0; \Omega = \frac{1}{H}\frac{\partial^2 \Psi}{\partial r^2} && \text{at the wall} \quad (r = 1), \\ &\frac{\partial W}{\partial r} = 0 && \text{at the centre} \quad (r = \theta = 0). \end{aligned}\right\} \tag{8}$$

Equations (3)–(5) are transformed into finite-difference expressions at the upper semicircular-section of the pipe because the flow is symmetrical about the X-axis. In the computation, extremely fine grids are required near the wall because of the very steep gradient of physical quantities. Here non-uniform grids, which are constructed by nodal points of 15–26, are used in the radial direction and uniform grids constructed by nodal points of 16–21 are applied in the circumferential direction. In the transformation into finite-difference expressions, the second-order central difference is used for all spatial derivatives. On the other hand, equi-interval timesteps, which amount to 720–5040 per cycle, are adopted except for low Womersley numbers. To advance the calculation with time increment, it is necessary to use the axial pressure gradient, $\partial P/\partial Z$, in terms of known variables W and Ψ at the preceding timestep. This pressure gradient can be obtained by integrating (3) over the cross-section (Takami, Sudo & Sumida 1984). The equations for W, Ω and Ψ are solved explicitly by the unsteady method similar to the procedure of Joseph, Smith & Adler (1975), the initial values of them being set to zero at all grid nodes. A run is terminated when the following iterative-error criterion is satisfied at all timesteps:

$$\frac{1}{mn} \sum_{i=1}^{m} \sum_{j=1}^{n} \left| 1 - \frac{F_{i,j}^{k-1}}{F_{i,j}^{k}} \right| < 10^{-4}, \tag{9}$$

where F is a representative of W, Ω and Ψ; k, m and n are the number of the

calculation cycle and of the grid node. Three to thirty-two iterations are required to achieve this criterion in our calculation.

The computations were carried out in a wide range of three parameters: the Womersley numbers $\alpha = 0 \sim 30$, the Dean numbers $D = 10 \sim 500$ and the radius ratios $Rc(= R/a) = 7.6 \sim 100$.

4. Results and discussion

Typical photographs are given in figure 3. In addition to the dimensionless parameters D and α, the phase in a cycle $\Theta(= \omega t)$ and the phase interval of the stroboscope irradiation $\Delta\Theta$ are entered for the photographs by method ①; the real time interval of the irradiation $\Delta t(= nT_p)$ is added for the photographs by method ②, T_p being the period of the oscillatory motion and n a positive integer. The left- and right-hand sides of the photographs correspond to the inner and outer walls of the pipe, respectively. Here we can classify the secondary flows into five types according to their flow mechanism and characteristics: (i) Dean circulation – type (I); (ii) deformed Dean circulation – type (II); (iii) intermediate circulation between Dean and Lyne – type (III); (iv) deformed Lyne circulation – type (IV); (v) Lyne circulation – type (V). The secondary flows of types (I) and (V), that is, the Dean and Lyne circulations, have been known since the works of Dean (1927, 1928) and Lyne (1970). Five types of secondary flow are illustrated schematically in figure 4.

The photographs are arranged on the α *vs.* D chart in figure 5 and the experimental conditions and others are listed in table 1. The letters in the left-hand column of the table correspond to those in figures 3 and 5. The solid lines in figure 5, which distinguish the flow patterns, are drawn on the basis of both experimental and numerical results.

Figure 6 displays the X-component profiles of the velocity on the Y-axis, which are constructed on the basis of several photographs under the same conditions, U being the instantaneous velocity and $\bar{U}$ the time-averaged velocity in a cycle. The positive values of U or $\bar{U}$ denote that the fluid moves toward the outer bend. The solid lines in figure 6 indicate the numerical results.

The locus of the centre of the secondary flow in a cycle is indicated in figure 7, of which the upper and lower half sections are concerned with the primary and secondary vortices, respectively. In these figures, the filled symbols show the experimental results, the open symbols express the numerical ones, and the solid and broken lines connecting the open symbols mean that the numerical results are obtained by methods ① and ②, respectively.

Figure 8 shows the secondary flow intensity defined in §4.2. The effects of the Womersley and Dean numbers on the secondary flow and the foundations of flow classification will be discussed in detail in the following sections.

4.1. *Mechanism of secondary flow generation*

4.1.1. *Flow for low Dean numbers* ($D \lesssim 100$)

When the Dean number is less than 100, the effects of the pipe curvature are not appreciable. Therefore, for the low Womersley numbers less than 5.5, where the viscous effects extend to the central region of the pipe, the centre of the spiral motion of the secondary flow exists almost at the central part of the semicircular section of the pipe as shown in figures 3(*a*, *b*) and 5(*q*) and it scarcely shifts during a cycle as seen in figure 7(*a*). This flow pattern is named type (I).

When the Womersley number goes up to about 10, the viscous effects become

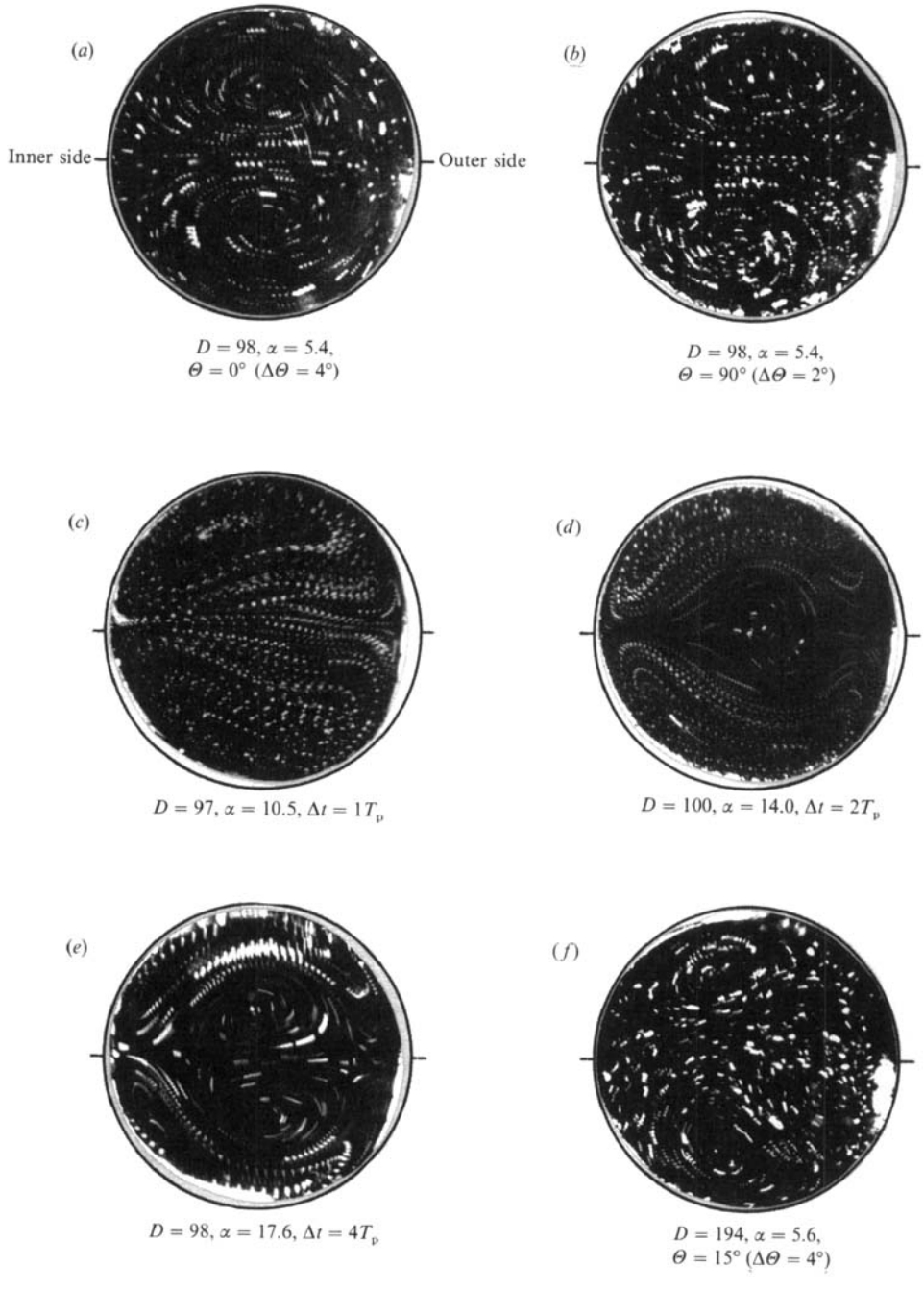

FIGURE 3(*a–f*). For caption see p. 198.

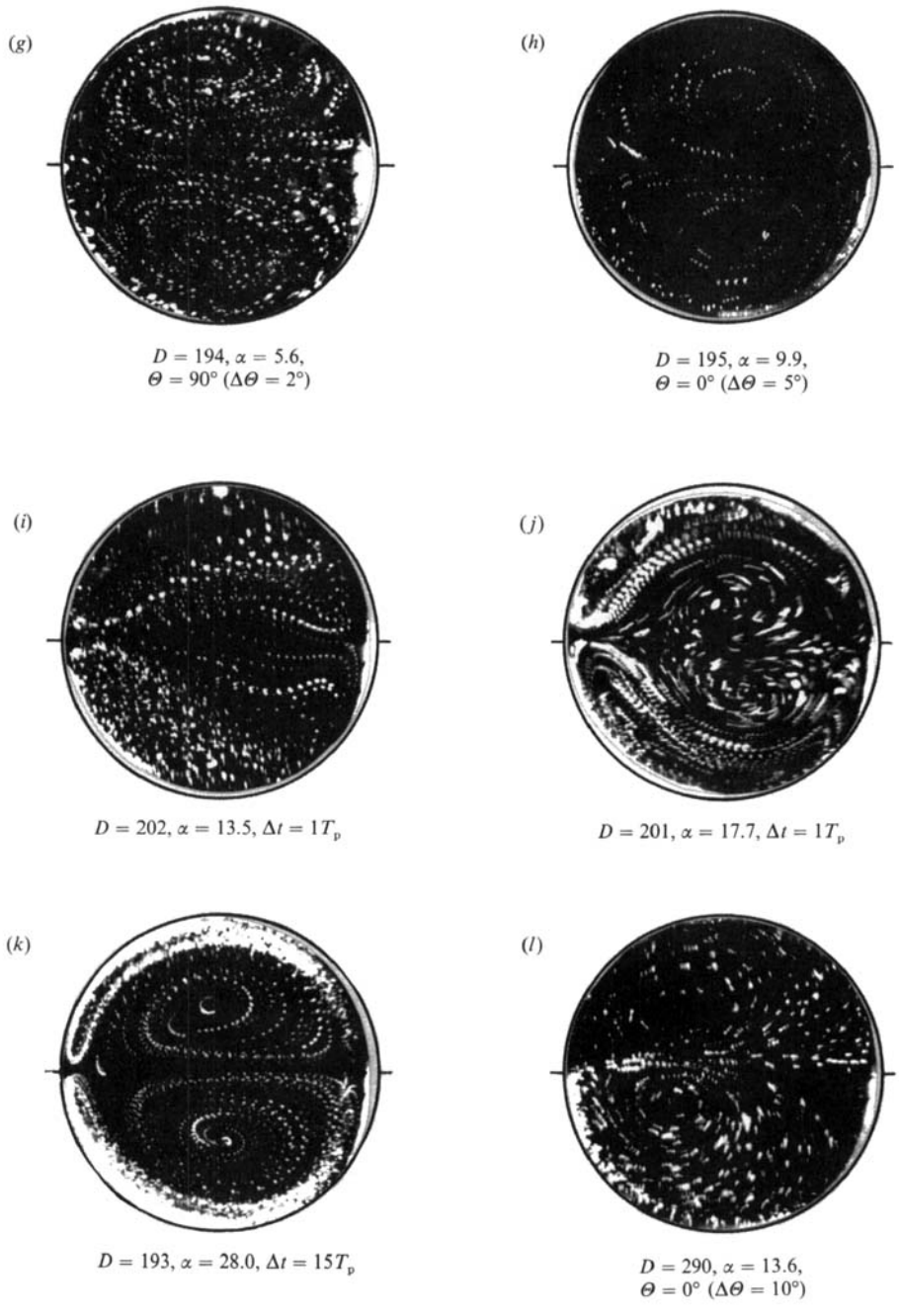

FIGURE 3(*g–l*). For caption see p. 198.

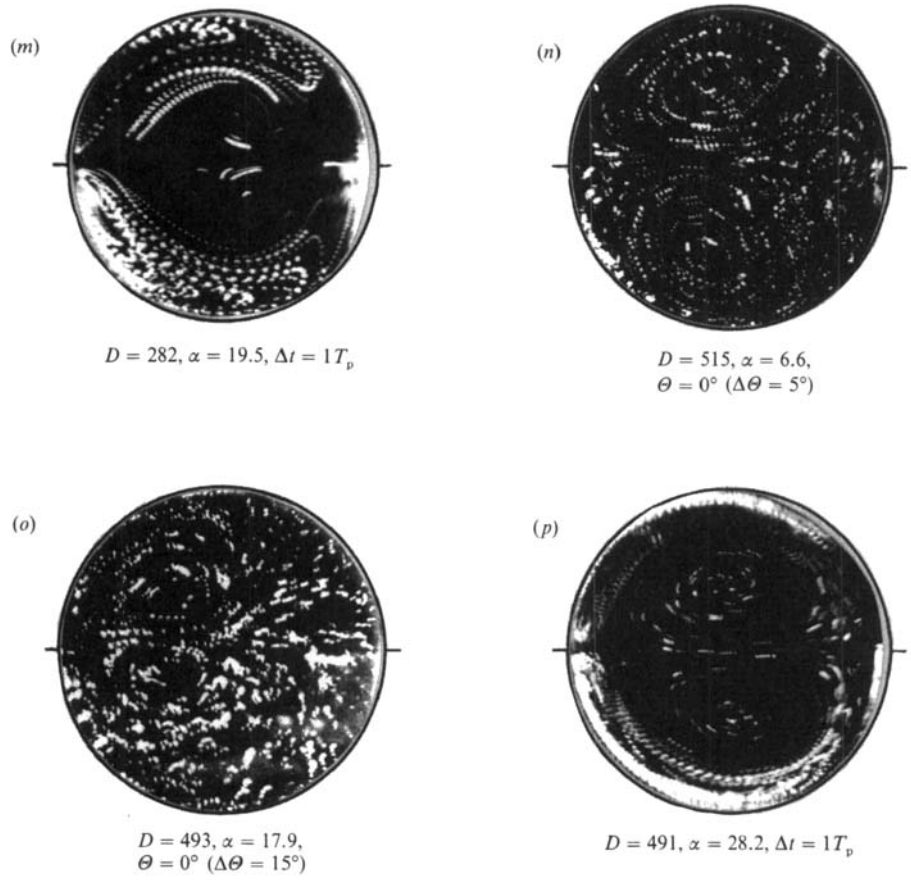

FIGURE 3. Photographs of secondary flow. The left- and right-hand sides of the photographs correspond to the inner and outer walls of the pipe, respectively. The experimental conditions are noted under the photographs.

restricted to the neighbourhood of the wall and the inertia effects increase relatively in the middle region of the pipe. Since the fluid in the middle region cannot follow obediently the variation of the axial pressure gradient compared to the fluid near the wall, the axial velocity has an annular profile which takes the form of a crest near the wall and the bottom in the middle part (Uchida 1956). In flows when the Womersley number is a little greater than 10, the axial velocity becomes nearly uniform in the central region of the pipe and the magnitude of the centrifugal force and the pressure gradient in the direction of the pipe curvature radius becomes roughly equal there. As a result, the fluid near the outer wall stops moving toward the wall and the secondary motion in the central part of the pipe weakens. In other words, the stagnant region of the secondary flow appears near the outer wall and the generation of the stagnant region pushes the vortices toward the upper and lower walls as seen in figures 3(*c*) and 5(*r*). This flow pattern is called type (II).

When the Womersley number increases slightly, the pressure gradient becomes superior to the centrifugal force in the central region of the pipe in a certain period of a cycle and the stagnant fluid near the outer wall moves toward the inside in this

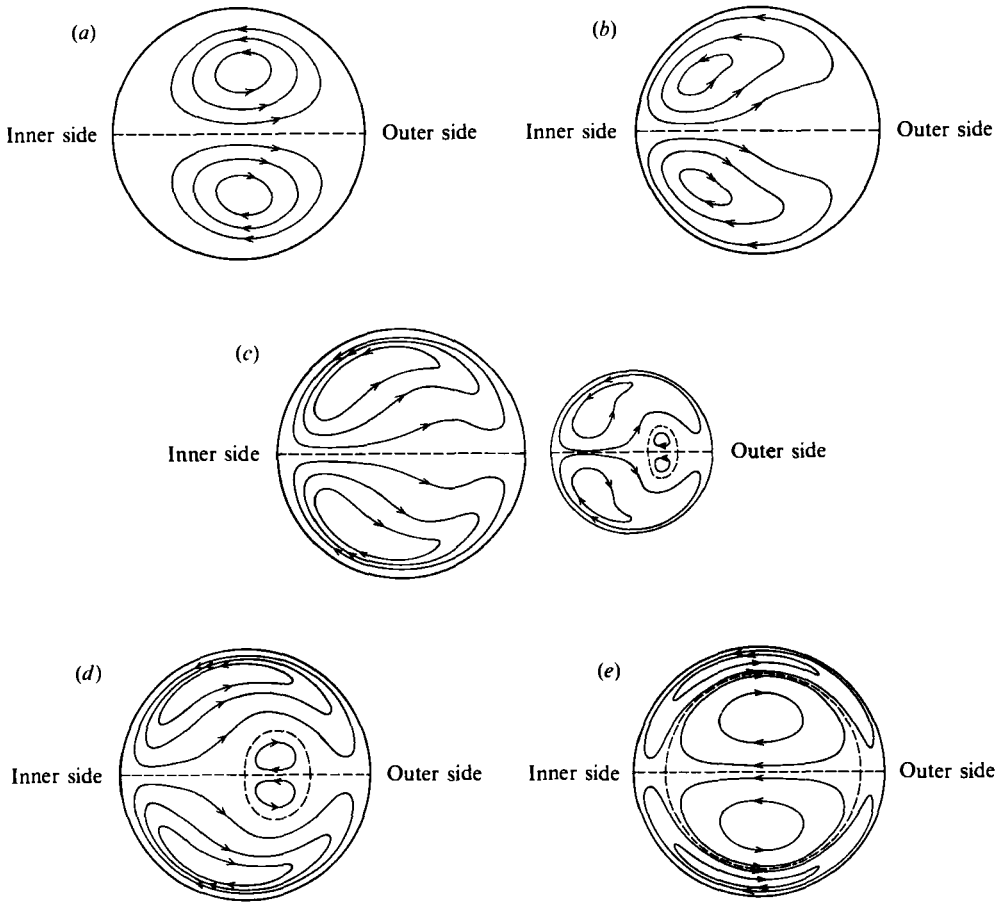

FIGURE 4. Schematic diagrams of the secondary flow patterns. (*a*) Dean circulation – type (I). See photographs (*a*), (*b*), (*f*), (*g*), (*h*), (*n*), (*q*), (*t*), (*u*) and (*x*) in figures 3 and 5. (*b*) Deformed Dean circulation – type (II). See photographs (*c*), (*l*), (*o*) and (*r*) in figures 3 and 5. (*c*) Intermediate circulation between Dean and Lyne circulations – type (III). Additional twin vortices are induced in a certain period of a cycle as drawn at the right-hand side. See photographs (*i*) and (*w*) in figures 3 and 5. (*d*) Deformed Lyne circulation – type (IV). See figure 3(*d*, *m*). (*e*) Lyne circulation – type (V). See photographs (*e*), (*j*), (*k*), (*p*), (*s*), (*v*) and (*y*) in figures 3 and 5.

period. As a result, an additional pair of vortices, which rotate in the direction opposite to that of the primary vortices, appears in the region near the outer wall for a short time. In this case, the secondary flow forms the flow pattern as shown in figure 4(*c*). Such a flow pattern belongs to type (III).

When the Womersley number is increased further, the additional twin vortices, whose cores are deviated slightly to the outside, can be observed in the central region throughout the cycle. This flow, shown in figures 3(*d*), 4(*d*) and 6(*a*)(iii), is referred to as type (IV), that is, the deformed Lyne circulation.

The Womersley number at which the two pairs of vortices begin to appear in a certain period of a cycle has been given as follows. Our numerical analysis gives $\alpha = 11$ that is indicated by the line A in figure 5. The theories of Lyne (1970), Zalosh & Nelson (1973) and Mullin & Greated (1980) give $\alpha \doteqdot 12.9$, 10.6 and $10 \sim 11$,

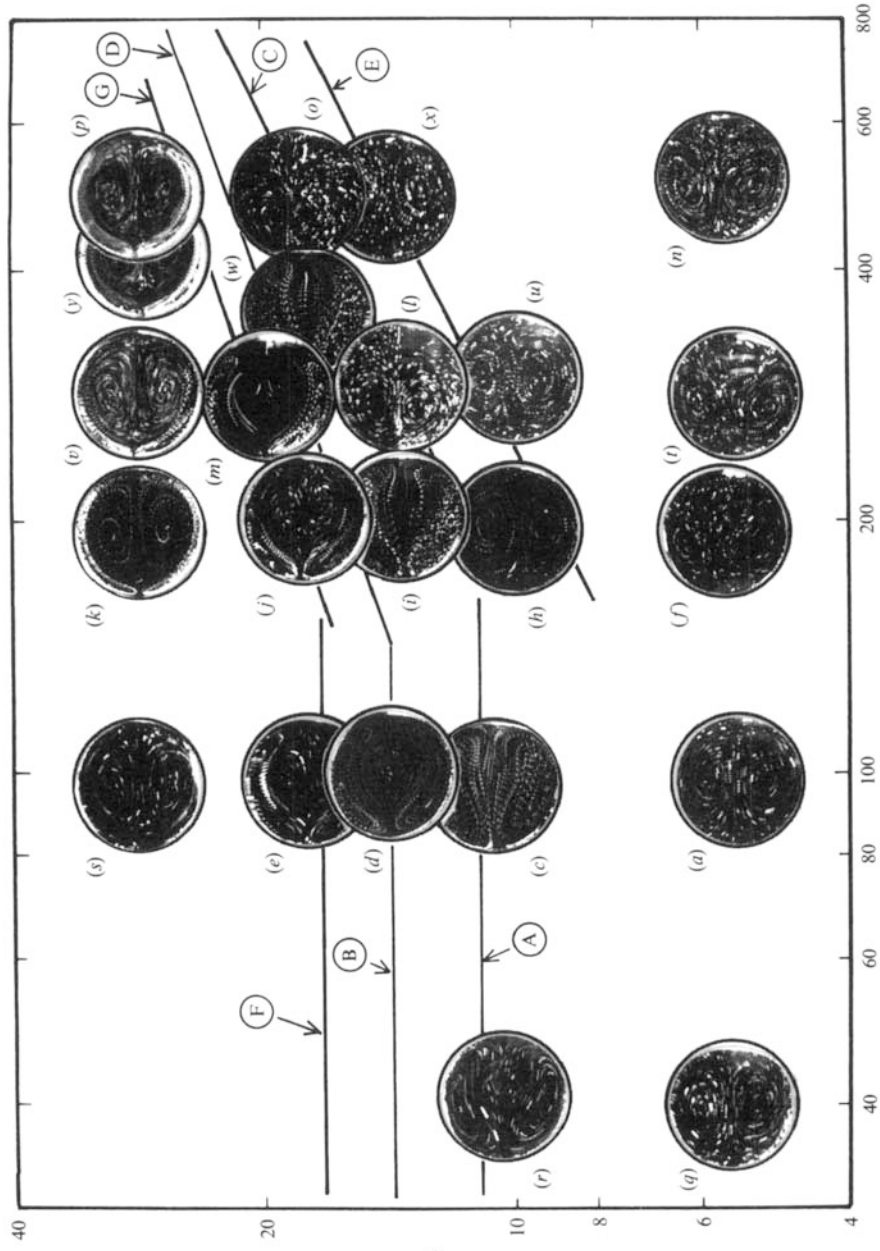

FIGURE 5. Secondary flow photographs arranged on α *vs.* D chart. The symbols (*a*) to (*y*) are referred to in table 1. The solid lines A–F distinguish the flow patterns: line A denotes $\alpha = 11$ at which the Lyne's motion appears in a certain period of a cycle and it indicates the boundary line between flow patterns (II) and (III) for $D \lesssim 100$; lines B and D are given by $\alpha = 14$ and (11) of the text and express the boundary lines between the flow patterns (III) and (IV); lines F and G are expressed by (12) of the text and show the boundary between (IV) and (V); line C is given by (10) of the text and shows the boundary between (II) and (III) for $D \gtrsim 200$; line E shows the boundary between (I) and (II) for $D \gtrsim 200$ and is expressed by (14) of the text.

respectively. The results of the present experiments have also proved these Womersley number values to be valid. Next, the lowest value of α at which the two pairs of vortices exist throughout a cycle is checked. The present numerical analysis gives $\alpha \doteqdot 14$, which is denoted by the line B in figure 5, and this is consistent with the values of 13.5 and 14.1 from the visualization experiments of Munson (1975) and Bertelsen (1975).

With a further increase in the Womersley number, the annular profile of the velocity is formed firmly and the viscous effects are restricted in the thin fluid layer near the wall. This means that the region of large axial velocity, which causes the primary vortices, moves nearer to the wall. Consequently, the primary vortices shift further toward the wall and the additional vortices occupy the central region of the section. In this flow pattern, both the vortices attenuate and the time-averaged velocity $\bar{U}$ decreases as seen in figures 3(*e*), 5(*s*), 6(*a*)(iv) and 7(*a*). This secondary flow is named type (V), which is known as the typical Lyne circulation.

4.1.2. *Flow for high Dean numbers* ($D \gtrsim 200$)

For Dean numbers more than 200, the centrifugal force exerted on the fluid becomes predominant in the whole region of the pipe cross-section except for the thin fluid layer on the wall. Therefore, the secondary flow pattern shows more complicated variation with Womersley number than in low Dean numbers.

For Womersley numbers less than 5.5, in which the centrifugal effects are predominant compared to the unsteady inertia effects, the secondary flow has a similar pattern to that of the steady flow except in the part of a cycle in the vicinity of $\Theta = 0°$. To put it concretely, the secondary flow behaves in a cycle as follows. The vortices exist in the inner region of the cross-section at the zero flow-rate phase and its vicinity as shown in figures 3(*f*, *n*) and 5(*t*) and their intensity is low; as the flow rate increases, the secondary flow grows and shifts its centres toward the upper and lower walls, as observed in the steady flow at the same Dean number. Thus the centres of the secondary flow move about during a cycle as seen in figure 7(*b*, *c*). On the whole, the X-component of the velocity varies in much the same phase with the flow rate as indicated in figure 6(*b*)(i), and so the profile of the axial flow becomes similar to that of the steady flow as mentioned above. The secondary flow in this case belongs to type (I).

When the Womersley number increases and the time required for the fluid to circulate in the cross-section approaches the same value as a period of the centrifugal force acting periodically on the fluid, π/ω, the secondary flow is intensified and the fluid, in plenty of momentum in the axial direction near the outer bend, is forced inwardly along the wall by the vivid secondary flow even in the decelerative phase, i.e. $\Theta \doteqdot 90 \sim 180°$ or $\Theta \doteqdot 270 \sim 360°$. As a result, the fluid near the inner wall is accelerated in the axial direction even in the low flow-rate phase and this makes strong secondary flow even at the minimum flow rate as seen in figures 3(*h*), 5(*u*, *x*) and 6(*b*)(ii). In this flow, the secondary flow velocity scarcely varies during a cycle and the cores of the vortices are held at a bit of the outside in the central region of the half cross-sections as shown in figures 7(*b*) and 7(*c*).

When the Womersley number increases a bit, the unsteady inertia effects come to predominate in the core region of the pipe and the axial velocity becomes nearly uniform there. This results in, as mentioned above, the balance of the centrifugal force and the pressure gradient of the pipe curvature radius direction in the central section. The balance of the forces in the core region stops the secondary flow from moving near the outer wall and makes the stagnant region of the secondary flow

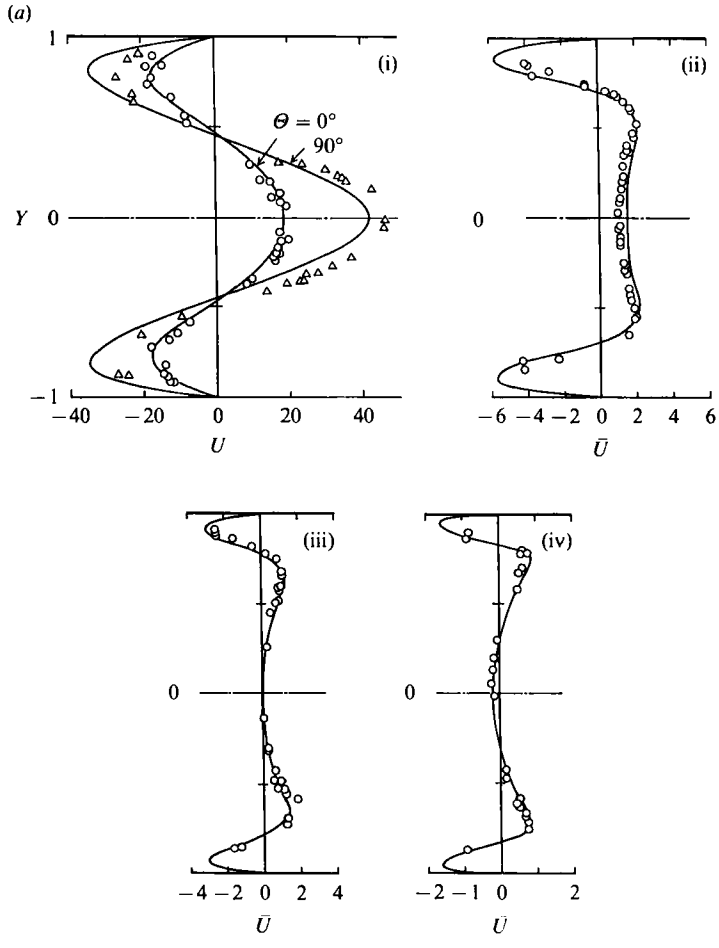

FIGURE 6(a). For caption see facing page .

there. This causes the vortices to shift towards the inner region, where the axial velocity variation is large in a cycle, as seen in figure 3(*l*, *o*). This secondary flow belongs to type (II).

In secondary flow of type (II), the unsteady inertia effect of the main flow is predominant in the central region of the pipe and the convective one of the secondary flow is dominant in the inner region, as mentioned already. Now a parameter, α^2/D, which means the ratio of the magnitude of the main flow inertia and that of the secondary flow, is made. The line C in figures 5 and 8 represents the relation between the Womersley and Dean numbers at which the pipe curvature effects on the flow resistance factor begin to be recognized and its expression is given as

$$\alpha^2/D = 0.655. \tag{10}$$

The intensity of the secondary flows begins to decrease suddenly over the line C as shown in figures 8 and 6(*b*)(iii), and the flow pattern changes to a great extent as seen in figure 5. That is, the less viscous region occupies the central part of the pipe because of an increase of the unsteady inertia effect, as stated in the previous

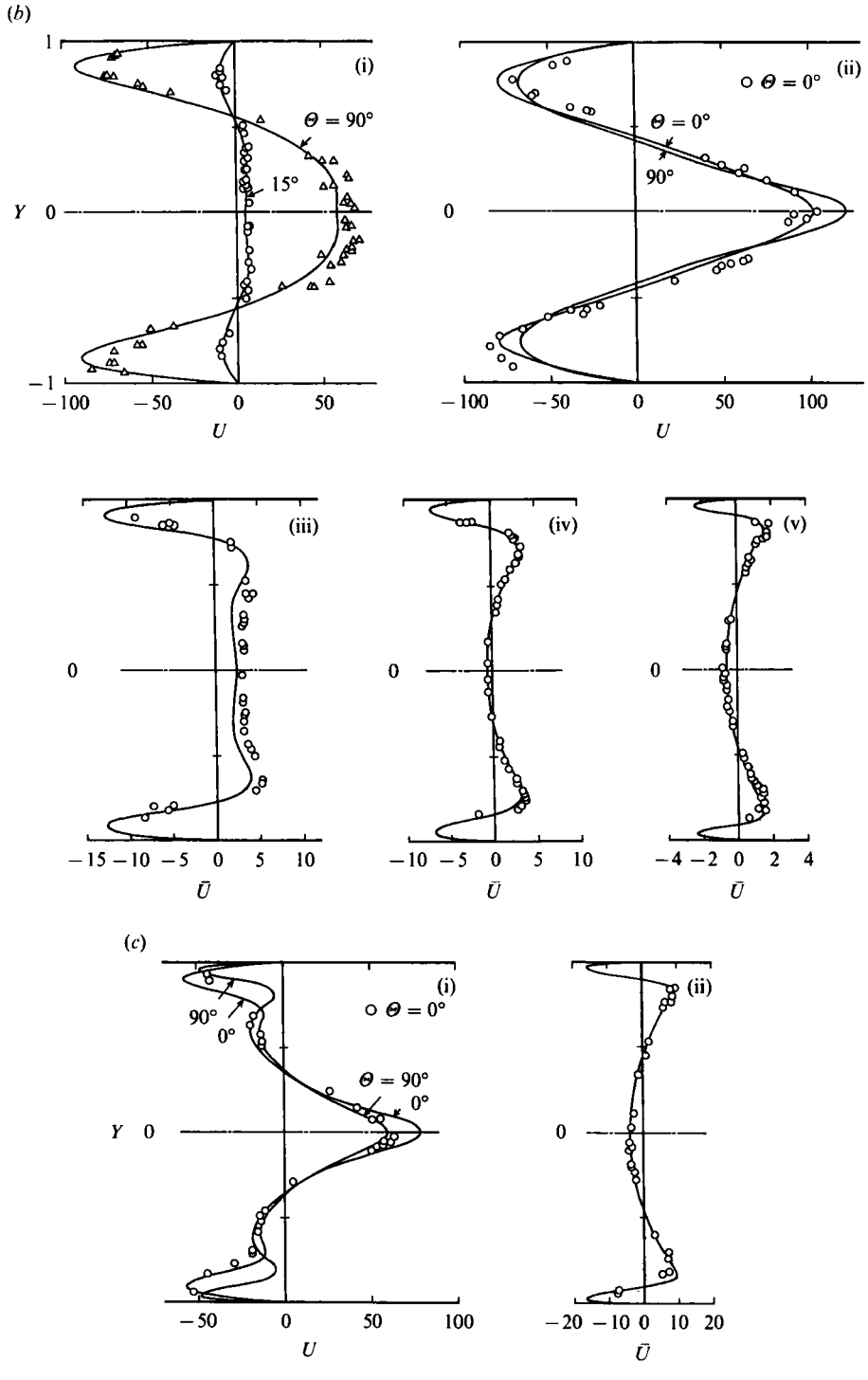

FIGURE 6. Profiles of the X-component of velocity on Y-axis. U and $\bar{U}$ are the instantaneous and time-averaged velocities respectively. The solid lines indicate the numerical results, and ○, △ the experimental ones. (*a*)(i) $\alpha = 5.4$, $D = 98$; (ii) $\alpha = 10.5$, $D = 97$; (iii) $\alpha = 14.0$, $D = 100$; (iv) $\alpha = 17.6$, $D = 9.8$. (*b*)(i) $\alpha = 5.6$, $D = 194$; (ii) $\alpha = 9.9$, $D = 195$; (iii) $\alpha = 13.5$, $D = 202$; (iv) $\alpha = 17.7$, $D = 201$; (v) $\alpha = 28.0$, $D = 193$. (*c*)(i) $\alpha = 17.9$, $D = 493$; (ii) $\alpha = 28.2$, $D = 491$.

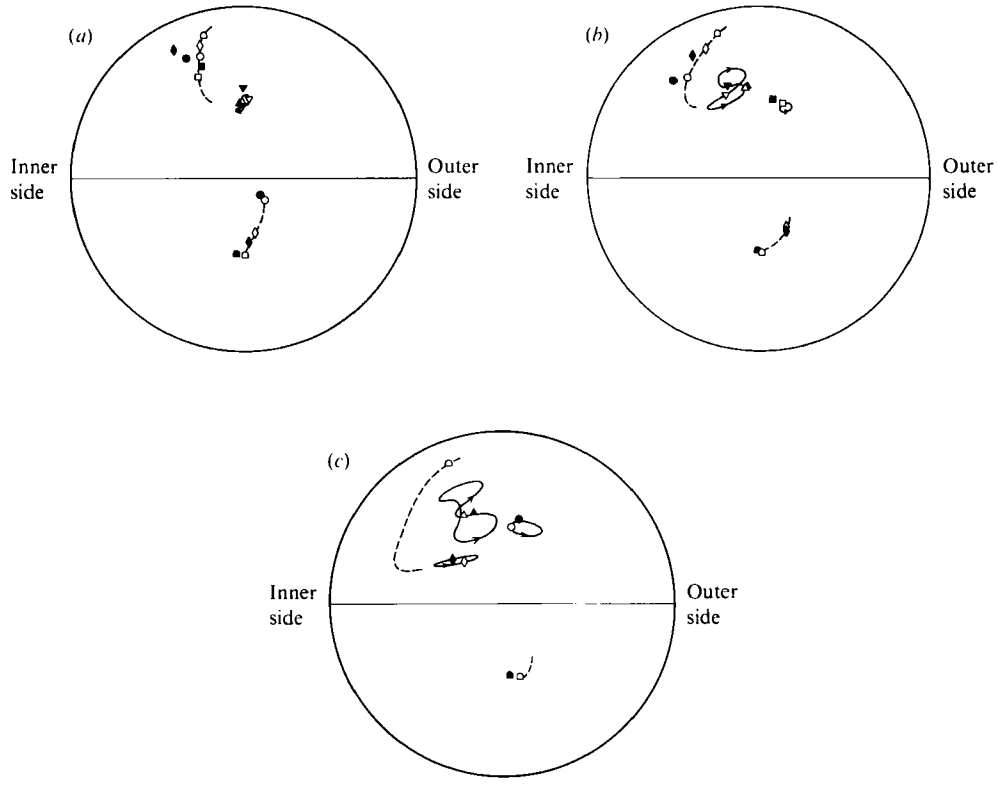

FIGURE 7. Locus of the centre of the secondary flow in a cycle. The primary and secondary vortices are shown in the upper and lower half sections of the figure, respectively. The solid and broken lines and open symbols show the numerical results, the filled symbols indicate the experimental ones. (*a*) $D \doteqdot 100$; △, ▽, $\alpha = 5.4$, $\Theta = 0°$ and 90° (instantaneous); □, ○, ◇, ⌂, $\alpha = 10.5$, 14.0, 17.6 and 28.1 (time-averaged). (*b*) $D \doteqdot 200$; △, ▽, $\alpha = 5.6$, $\Theta = 15°$ and 90° (instantaneous); □, $\alpha = 9.9$, $\Theta = 0°$ (instantaneous); ○, ◇, ⌂, $\alpha = 13.5$, 17.7 and 28.0 (time-averaged). (*c*) $D \doteqdot 500$; △, ○, ◇, $\Theta = 0°$, $\alpha = 5.6$, 14.0 and 17.9 (instantaneous); ⌂, $\alpha = 28.2$ (time-averaged).

paragraph, and the secondary vortices come to appear in this region at a part of a cycle, the cores of the vortices shifting near the upper and lower walls as shown in figures 3(*i*), 5(*w*) and 7(*b*, *c*). This secondary flow belongs to type (III).

When the Womersley number increases further, the additional vortices exist all through a cycle and secondary flow of type (IV) is formed. The secondary flow pattern changes from type (IV) to type (V) with an increase of the Womersley number, as seen in figures 3(*j*, *k*, *m*, *p*) and 5(*y*, *v*), for the same reasons as explained for the low Dean numbers.

The lines of B and D in figures 5 and 8 show the Womersley number or the relation of the Womersley and Dean numbers at which the time-averaged velocity in the X-direction at the pipe axis changes its direction, that is, the secondary flow changes its pattern from type (III) to (IV). These are expressed as

$$\left.\begin{aligned} \alpha &= 14 \quad (D \lesssim 100), \\ \alpha^{2.8}/D &= 11.3 \quad (D \gtrsim 200). \end{aligned}\right\} \tag{11}$$

In addition, lines H and G denote the Womersley number or the relations of

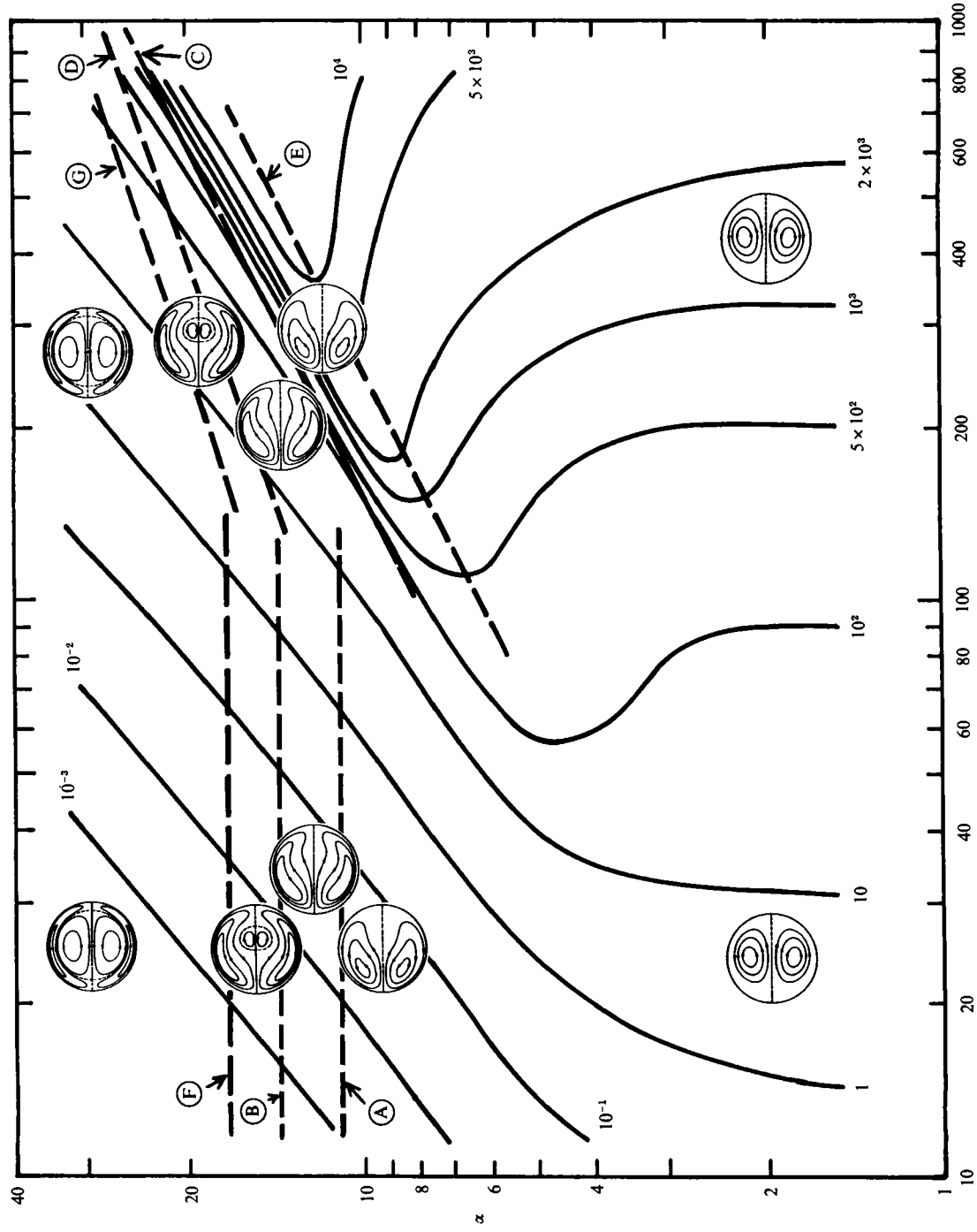

FIGURE 8. Equi-kinetic energy lines of the secondary flow. ——, numerical results. – – –, A–F distinguish the flow patterns, and the descriptions are referred to in the caption to figure 5.

parameters at which the time-averaged velocity toward the inner bend at the pipe axis takes the maximum value and are expressed as

$$\left.\begin{aligned} \alpha &= 17 \quad (D \lesssim 100), \\ \alpha^3/D &= 30 \quad (D \gtrsim 200). \end{aligned}\right\} \tag{12}$$

The lines H and G are considered as the rough border lines between secondary flow of type (IV) and (V).

For the intermediate Dean numbers ranging from 100 to 200, the numerical solution shows that the secondary flow pattern changes roughly in the same manner as observed for the low Dean numbers ($D \lesssim 100$).

4.2. *Kinetic energy of the secondary flow*

In curved pipe oscillatory flow, as stated until now, two or four vortices are induced in the cross-section. Here we use the kinetic energy as a measure of the intensity of the secondary flows. It is defined as

$$S = 2a^2 e/(\rho \nu^2) = \frac{1}{2\pi^2} \int_0^{2\pi} \int_{-\pi}^{\pi} \int_0^1 (U^2 + V^2)\, r \, \mathrm{d}r \, \mathrm{d}\theta \, \mathrm{d}\Theta, \tag{13}$$

where V is the dimensionless velocity of the Y-direction and e denotes the mean of the secondary flow velocity squared. Therefore S is the time- and space-averaged value of the kinetic energy of the secondary flow in a cycle.

Curves of constant-S are shown in figure 8. In the figure, the boundaries classifying the secondary flow are shown with the broken lines A–G and the schematic vortex figures are inserted. The line E denotes the flow condition at which the kinetic energy of the secondary flow becomes maximum and is expressed as

$$\alpha^2/D = 0.41. \tag{14}$$

It forms the boundary between type (I) and (II) of the secondary flow at high Dean numbers. For low Womersley numbers less than 2, at which the flow pattern shows type (I), S increases in proportion to D^2. On the other hand, S varies approximately with $\alpha^{-5}D^4$ under the condition that the inertia effects prevail compared with the curvature effects; this condition occurs in the regions above the line A for $D \lesssim 100$ and above the line D for $D \gtrsim 200$ in figures 5 and 8. For high Dean numbers, i.e. $D \gtrsim 200$, S increases at first with an increase of Womersley number and then decreases at Womersley numbers higher than a certain value. This indicates the boundary across which the flow pattern changes rapidly from type (II) to (IV) through (III).

5. Conclusions

The measurements and calculations reported here reveal several features of secondary flow. An important conclusion induced in the developed oscillatory laminar flow through a circular curved pipe is that the secondary flow or vortical motion is classifiable into five patterns: (i) Dean circulation, (ii) deformed Dean circulation, (iii) intermediate circulation between Dean and Lyne circulations, (iv) deformed Lyne circulation and (v) Lyne circulation. The boundaries classifying the flow pattern are expressed in terms of the Womersley number or of the Womersley and Dean numbers according to the magnitude of the Dean number.

The kinetic energy of the secondary flow, S, increases with D^2 for low Womersley

numbers ($\alpha \lesssim 2$) and with $\alpha^{-5}D^4$ for high Womersley numbers which are $\alpha \gtrsim 11$ at $D \lesssim 100$ and $\alpha \gtrsim (11.3D)^{1/2.8}$ at $D \gtrsim 200$. However, S decreases at the Womersley number higher than the value given by the expression of $\alpha^2/D \doteqdot 0.655$.

REFERENCES

ADLER, M. 1934 Strömung in gekrümmten Rohren. *Z. Angew. Math. Mech.* **5**, 257–275.

AKIYAMA, M. & CHENG, K. C. 1971 Boundary vorticity method for laminar forced convection heat transfer in curved pipes. *Intl J. Heat Mass Transfer* **14**, 1659–1675.

AUSTIN, L. R. & SEADER, J. D. 1973 Fully developed viscous flow in coiled circular pipes. AIChEJ. **19**, 85–94.

BARUA, S. M. 1963 On secondary flow in stationary curved pipes. *Q. J. Mech. Appl. Maths* **16**, 61–77.

BERGER, S. A., TALBOT, L. & YAO, L. S. 1983 Flow in curved pipes. *Ann. Rev. Fluid Mech.* **15**, 461–512.

BERTELSEN, A. F. 1975 An experimental investigation of low Reynolds number secondary streaming effects associated with an oscillating viscous flow in a curved pipe. *J. Fluid Mech.* **70**, 519–527.

BERTELSEN, A. F. & THORSEN, L. K. 1982 An experimental investigation of oscillatory flow in pipe bends. *J. Fluid Mech.* **118**, 269–284.

CHANG, L. J. & TARBELL, J. M. 1985 Numerical simulation of fully developed sinusoidal and pulsatile (physiological) flow in curved tubes. *J. Fluid Mech.* **161**, 175–198.

CHRISTOV, C. & ZAPYRANOV, Z. 1980 Oscillatory fully developed viscous flow in a toroidal tube. *Comp. Methods Appl. Mech. Engng* **22**, 49–58.

COLLINS, W. M. & DENNIS, S. C. R. 1975 The steady motion of a viscous fluid in a curved tube. *Q. J. Mech. Appl. Maths* **28**, 133–156.

DEAN, W. R. 1927 Note on the motion of fluid in a curved pipe. *Phil. Mag.* **4**(7), 208–223.

DEAN, W. R. 1928 The stream-line motion of fluid in a curved pipe. *Phil. Mag.* **5**(7), 673–695.

ECKMANN, D. M. & GROTBERG, J. B. 1988 Oscillatory flow and mass transport in a curved tube. *J. Fluid Mech.* **188**, 509–527.

GREENSPAN, A. D. 1973 Secondary flow in a curved tube. *J. Fluid Mech.* **57**, 167–176.

ITO, H. 1969 Laminar flow in curved pipes. *Z. Angew. Math. Mech.* **11**, 653–663.

JOSEPH, B., SMITH, E. P. & ADLER, R. J. 1975 Numerical treatment of laminar flow in helically coiled tubes of square cross section. Part 1. *AIChE J.* **21**, 965–974.

KALB, C. E. & SEADER, J. D. 1972 Heat and mass transfer phenomena for viscous flow in curved circular tubes. *Intl J. Heat Mass Transfer* **15**, 801–817.

LI, C. H. 1976 A note in comment on 'Analysis of steady laminar flow of an incompressible newtonian fluid through curved pipes of small curvature'. *Trans. ASME* I: *J. Fluids Engng* **98**, 323–325.

LYNE, W. H. 1970 Unsteady viscous flow in a curved pipe. *J. Fluid Mech.* **45**, 13–31.

MULLIN, T. & GREATED, C. A. 1980 Oscillatory flow in curved pipes. Part 2. *J. Fluid Mech.* **98**, 397–416.

MUNSON, B. R. 1975 Experimental results for oscillatinf flow in a curved pipe. *Phys. Fluids* **18**, 1607–1609.

SANKARAIAH, M. & RAO, Y. V. M. 1973 Analysis of steady laminar flow of an incompressible newtonian fluid through curved pipes of small curvature. *Trans. ASME* I: *J. Fluids Engng* **95**, 75–80.

SMITH, F. T. 1976 Steady motion with a curved pipe. *Proc. R. Soc. Lond.* A **347**, 345–370.

TAKAMI, T., SUDO, K. & SUMIDA, M. 1984 Pulsating flow in curved pipes. 1st Report. *Bull. JSME* **27**-234, 2706–2713.

TARBELL, J. M. & SAMUELS, M. R. 1973 Momentum and heat transfer in helical coils. *Chem. Engng J.* **5**, 117–127.

TOPAKOGLU, H. C. 1967 Steady laminar flows of an incompressible viscous fluid in curved pipes. *J. Math. Mech.* **16**, 1321–1337.

TRUESDELL, L. C. & ADLER, R. J. 1970 Numerical treatment of fully developed laminar flow in helically coiled tubes. *AIChE J.* **16**, 1010–1015.

UCHIDA, S. 1956 The pulsating viscous flow superposed on the steady laminar motion of incompressible fluid in a circular pipe. *Z. Angew. Math. Phys.* **7**, 403–422.

VAN DYKE, M. 1978 Extended stokes: laminar flow through a loosely coiled pipe. *J. Fluid Mech.* **86**, 129–145.

ZALOSH, R. G. & NELSON, W. G. 1973 Pulsating flow in a curved tube. *J. Fluid Mech.* **59**, 693–705.